Surface tension of water and acid gases from Monte Carlo simulations

A. Ghoufi,[1] F. Goujon,[2] V. Lachet,[1] and P. Malfreyt[2,a)]
[1]*IFP, 1-4 Av. de Bois Préau, 92852 Rueil Malmaison Cedex, France*
[2]*Laboratoire de Thermodynamique des Solutions et des Polymères, UMR 6003 CNRS, Université Blaise Pascal, 63177 Aubière Cedex, France*

(Received 8 November 2007; accepted 11 March 2008; published online 21 April 2008)

We report direct Monte Carlo (MC) simulations on the liquid-vapor interfaces of pure water, carbon dioxide, and hydrogen sulfide. In the case of water, the recent TIP4P/2005 potential model used with the MC method is shown to reproduce the experimental surface tension and to accurately describe the coexistence curves. The agreement with experiments is also excellent for CO_2 and H_2S with standard nonpolarizable models. The surface tensions are calculated by using the mechanical and the thermodynamic definitions via profiles along the direction normal to the surface. We also discuss the different contributions to the surface tension due to the repulsion-dispersion and electrostatic interactions. The different profiles of these contributions are proposed in the case of water. © *2008 American Institute of Physics*. [DOI: 10.1063/1.2904458]

I. INTRODUCTION

The risks associated with climate change have been the subject of much debate in recent years. Today, most experts think that these risks are real and directly linked to the increase of the emission of greenhouse gases, especially CO_2. Among the various options for mitigating these emissions, large-scale storage of CO_2 into underground formations such as deep saline aquifers or depleted oil and gas fields is a promising option.[1] The success of such CO_2 sequestration operations largely depends on safety concerns. Indeed, CO_2 may escape from the formation through different possible pathways, such as abandoned wells, faults or fractures, or through the caprock, which is a low permeability media saturated with water that lies at the top of the reservoir. This risk of leakage through the caprock is largely governed by the fluid-fluid and the fluid-rock interfacial interactions. One of these interactions is the CO_2-water interfacial tension, which not only influences the flow process but also controls the capillary-sealing efficiency,

$$p_c = p_{CO_2} - p_{H_2O} = 2\gamma\cos(\theta)/R,$$

where p_c is the capillary pressure in the saturated water caprock, γ is the water-CO_2 interfacial tension, R is the largest connected pore throat in the caprock, and θ is the contact angle. Capillary breakthrough occurs when the overpressure, i.e., the difference between the gas pressure in the reservoir and the water pressure in the caprock, exceeds the capillary pressure p_c. For instance, if $R \approx 0.01$ μm and if the water is assumed to be a good wetting fluid ($\theta \approx 0$), this capillary pressure is about 10 MPa if $\gamma \approx 50$ mN m^{-1}, but is only about 2 MPa if $\gamma \approx 10$ mN m^{-1}. Proper understanding and modeling of these interfacial properties are, thus, essential in assessing the suitability and the safety of CO_2 storage sites. These concerns will also be encountered in the case of acid gas reinjection into deep reservoirs, i.e., reinjection of H_2S and CO_2 mixtures resulting from the treatment of natural gases with a high H_2S content. This acid gas reinjection is a studied solution for acid gases disposal, which could be an attractive alternative to the H_2S transformation into elementary sulfur from an economic point of view.

Gas-water interfacial tensions are, thus, required for the design of such acid gas reinjection projects. Some experimental values of water-CO_2 interfacial tension have been reported by several authors since 1957 and a complete literature survey has been proposed in 2002 by Hebach *et al.*[2] The reported data indicate, however, a lack of values in the case of extreme pressure and temperature conditions. Concerning H_2S-water systems, very few data are available in the literature, and they mostly correspond to a gaseous H_2S phase,[3,4] i.e., at pressures much lower than the ones encountered in deep reservoirs. The design of reinjection projects of CO_2 or H_2S in deep reservoirs is, thus, hampered by this lack of experimental data of interfacial tension, and the extensive measurement of these would be too costly because of the toxicity and corrosiveness of these gases, particularly H_2S.

As far as modeling is concerned, several methods are available for the calculation of surface tensions of simple fluids. Most of them are correlative methods using the parachor theory[5,6] or the corresponding state principle.[7,8] Macroscopic models have also been developed that explicitly consider the concentration gradient at the interface.[9–12] However, when dealing with strongly nonideal mixtures, such methods have a limited predictive capacity, especially in the case of systems baring polar or amphiphilic components that are expected to preferentially locate at the interface.

In this context of a lack of experimental data, coupled with the insufficiency of quantitative prediction methods, we plan to use molecular simulation, more specifically Monte Carlo (MC) simulations, to assess interfacial study of water-CO_2 and water-H_2S mixtures and to get more fundamental insight into these interfacial phenomena. The development of a molecular simulation technique able to account

a)Author to whom correspondence should be addressed. Electronic mail: patrice.malfreyt@univ-bpclermont.fr.

 © 2008 American Institute of Physics

Downloaded 04 Jul 2008 to 194.214.132.32. Redistribution subject to AIP license or copyright; see http://jcp.aip.org/jcp/copyright.jsp

for the interfacial effects of polar pure components, such as CO_2, H_2S, and H_2O, is a first step toward the study of these more complex systems of industrial interest.

While much progress has already been made toward the molecular simulation of a two-phase system with an explicit interface, the nonuniformity of the local density along the direction normal to the surface gives rise to important issues concerning the truncation procedures involved in the calculation of the potential and force,[13,14] the long range correction (LRC) expressions used for the correction of the surface tension,[14] and the methodology used to account for the Coulombic interactions.[15–17] An inconsistent treatment of the truncation procedures has led to conflicting results of surface tension between MC and molecular dynamics (MD) methods. These problems of truncations have been illustrated for Lennard-Jones (LJ) fluids[13] and for *n*-alkanes.[18,14] As expected from a statistical point of view, it was shown that the MC and MD methods gave the same surface tension values on the condition that the discontinuities in force and energy equations be removed. In fact, the MC calculations carried out with a truncated potential cannot be compared to MD calculated by using a truncated force. The truncated force used in MD does not correspond to the truncated potential used in MC because the potential is not differentiable at the cutoff value. It means that the MC and MD calculations are carried out with different potential models. The solution[13] consists in either adding a δ function to the force taking into account the discontinuous change in the potential energy at the cutoff or using a potential truncated via a polynomial function that makes the first and second derivatives of the potential continuous at the cutoff.[19,14] The truncation of the potential is also relevant in the operational expressions of the surface tension: some expressions use the derivative of the potential and others make only use of the configurational energy. We have also established[14] that the different operational expressions of the surface tension lead to the same value under the condition that the discontinuity of the potential at the cutoff distance must be cancelled. The main conclusions that we can draw from these works[13,14,19] are as follows: the truncation of interactions has significant consequences on the equilibrium thermodynamic properties on a two-phase system; nevertheless, MC and MD methods exactly give the same interfacial properties with a consistent treatment of the truncation procedures.

Before calculating the surface tensions of water-H_2S and water-CO_2 binary systems, we focus our attention on the calculation of the surface tension of the liquid-vapor equilibria of pure components for water, hydrogen sulfide, and carbon dioxide molecules using MC simulations. We propose here to use the TIP4P/2005 model[19] in conjunction with the MC method to compare the calculated surface tension with the results obtained from MD simulations[20] and with experimental data.

We begin in Sec. II by describing the potential and methodology used. We complete this section with a brief summary of the operational expressions used for the calculation of both the intrinsic and LRC parts of the surface tension. We divide the discussion of our results into two parts: the comparison of the calculated surface tension of pure water, H_2S, and CO_2 with the experimental values is proposed in Sec. III A and the validation of the methodology used is discussed in Sec. III B. Section IV contains our conclusions and presents the future work.

TABLE I. The Lennard-Jones well depth ϵ and size σ, partial charges q, and geometry of the H_2O (Ref. 19), CO_2 (Ref. 21), and H_2S (Ref. 22) molecules; k_B is Boltzmann's constant.

TIP4P/2005 H_2O			
	σ (Å)	ϵ/k_B (K)	Charge (e)
O	3.1589	93.2	0
H	0	0	0.5564
M	0	0	−1.1128
OH distance (Å)			0.9572
H–O–H angle (deg)			104.52
OM distance (Å)			0.1546
EPM2 CO_2			
	σ (Å)	ϵ/k_B (K)	Charge (e)
C	2.757	28.129	+0.6512
O	3.033	80.507	−0.3256
C═O distance (Å)			1.149
O═C═O angle (deg)			180
H_2S			
	σ (Å)	ϵ/k_B (K)	Charge (e)
S	3.73	250	0.40
H	0	0	0.25
M	0	0	−0.90
SH distance (Å)			1.340
H–S–H angle (deg)			92
SM distance (Å)			0.1862

II. SIMULATION METHODOLOGY

A. Potential model

Water is modeled by using the four-point (TIP4P/2005) model.[19] Carbon dioxide molecule is represented by using the rigid version of the EPM2 intermolecular potential of Harris and Yung,[21] and hydrogen sulfide molecule is modeled by using the potential proposed by Kristof and Liszi.[22] The reader is directed to Table I for details of each potential model.

The total configurational energy of the systems formed by N molecules without any intramolecular interactions consists of intermolecular interactions modeled by LJ 6-12 sites, electrostatic point charges, and a LRC contribution,

$$U = U_{\mathrm{LJ}} + U_{\mathrm{ELEC}} + U_{\mathrm{LRC}}. \quad (1)$$

The intermolecular interactions due to the repulsion-dispersion interactions are computed by using the truncated LJ potential,

Downloaded 04 Jul 2008 to 194.214.132.32. Redistribution subject to AIP license or copyright; see http://jcp.aip.org/jcp/copyright.jsp

TABLE II. Dimensions of the box (Å), cutoff radius (r_c) (Å), and values of the reciprocal lattice wavelength vectors (Å^{-1}).

	H_2O	CO_2	H_2S
$L_x=L_y$	19.7	25.4	24.4
L_z	100	150.8	149.1
r_c	9.8	12.0	12.0
$\lvert h_x^{\max}\rvert=\lvert h_y^{\max}\rvert$	7	9	9
$\lvert h_z^{\max}\rvert$	33	41	41

$$U_{\mathrm{LJ}}=\sum_{i=1}^{N-1}\sum_{j>i}^{N}\sum_{a=1}^{N_i}\sum_{b=1}^{N_j}u_{\mathrm{LJ}}(r_{iajb})=\sum_{i=1}^{N-1}\sum_{j>i}^{N}\sum_{a=1}^{N_i}\sum_{b=1}^{N_j}4\epsilon_{ab}\left[\left(\frac{\sigma_{ab}}{r_{iajb}}\right)^{12}-\left(\frac{\sigma_{ab}}{r_{iajb}}\right)^{6}\right], \tag{2}$$

where r_{iajb} is the distance between atom a in molecule i and atom b in molecule j, ϵ_{ab} is the energy parameter of the interaction, and σ_{ab} is the LJ core diameter. N_i is the number of atoms in the molecule i. The LJ parameters for the interactions between unlike sites are calculated by using the Lorentz–Berthelot combining rules

$$\epsilon_{ab}=(\epsilon_{aa}\epsilon_{bb})^{1/2},\quad \sigma_{ab}=\tfrac{1}{2}(\sigma_{aa}+\sigma_{bb}). \tag{3}$$

In addition to the LJ interactions, the total electrostatic potential calculated by using the Ewald sum method[15,23–25] for a box with orthogonal axis is written as

$$U_{\mathrm{ELEC}}=\frac{1}{2\epsilon_0 V}\sum_{k\neq 0}Q(h)S(\mathbf{h})S(-\mathbf{h})+\frac{1}{8\pi\epsilon_0}\sum_i\sum_a\sum_{j\neq i}q_{ia}\sum_b q_{jb}\,\mathrm{erfc}(\alpha r_{iajb}/r_{iajb})-\frac{\alpha}{4\pi^{3/2}\epsilon_0}\sum_i\sum_a q_{ia}^2-\frac{1}{8\pi\epsilon_0}\sum_i\sum_a\sum_{b\neq a}\frac{q_{ia}q_{ib}}{r_{iaib}}\,\mathrm{erf}(\alpha r_{iaib}), \tag{4}$$

where erfc(x) is the complementary error function and erf(x) is the error function. α is chosen so that only pair interactions in the central cell need to be considered in evaluating the second term in Eq. (4). The functions $S(\mathbf{h})$ and $Q(h)$ are defined by using Eqs. (5) and (6), respectively,

$$S(\mathbf{h})=\sum_i\sum_a q_{ia}\exp(i\mathbf{h}\,.\,\mathbf{r_{ia}}), \tag{5}$$

$$Q(h)=\frac{1}{h^2}\exp\left(-\frac{h^2}{4\alpha^2}\right), \tag{6}$$

where the reciprocal lattice vector $\mathbf{h}$ is defined as $\mathbf{h}=2\pi(l/L_x,m/L_y,n/L_z)$, where l,m,n take values of $0,\pm1,\pm2,\ldots,\pm\infty$. The reciprocal space sum is truncated at an ellipsoidal boundary at the vector $|\mathbf{h}^{\max}|$. The values of the components of the maximum reciprocal lattice vector $|\mathbf{h}^{\max}|$ are given in Table II for each system with the convergence factor[26] $\alpha=2\pi/L_x$.

TABLE III. Average energy contributions (kJ mol^{-1}) calculated from the repulsion-dispersion (U_{LJ}), long range correction (U_{LRC}), Ewald real space (U_R), and Ewald reciprocal (U_K) terms. U represents the sum of the different contributions. The different energy contributions are divided by the number of molecules of the simulation cell. The subscripts give the accuracy of the last decimal(s), i.e., 8.6_3 means 8.6 ± 0.3.

U_{LJ}	U_{LRC}	U_R	U_K	U
Water, TIP4P/2005, $T=298$ K				
8.6_3	−0.11	-54.1_5	0.32_2	-45.3_8
Hydrogen sulfide, $T=232$ K				
-11.6_1	−0.40	-4.8_1	0.17_1	-16.6_3
Carbon dioxide, $T=228$ K				
-8.2_2	−0.14	-2.4_1	0.15_1	-10.6_3

As the geometry of the system shows an heterogeneity along the axis normal to the interface (z axis), we calculate the LRC to the repulsion-dispersion energy as a function of z_k by splitting the cell into slabs of width δz. The total LRC energy U_{LRC} is then calculated by summing up all the local contributions of each slab. The U_{LRC} term is then added in the total energy of the system to be used in the Metropolis scheme. The LRCs to the total energy within each kth slab are defined by two parts,[27]

$$U_{\mathrm{LRC}}=\sum_{i=1}^{N_s}u_{lrc}(z_k)=\sum_{i=1}^{N_s}(u_{lrc}^{(1)}(z_k)+u_{lrc}^{(2)}(z_k))\quad\text{with}$$

$$u_{lrc}^{(1)}(z_k)=\frac{8\pi}{3}\rho(z_k)^2V_s\sum_{a=1}^{N_i}\sum_{b=1}^{N_j}\epsilon_{ab}\left[1/3\left(\frac{\sigma_{ab}^{12}}{r_c^9}\right)-\left(\frac{\sigma_{ab}^{6}}{r_c^3}\right)\right], \tag{7}$$

$$u_{lrc}^{(2)}(z_k)=\pi\rho(z_k)V_s\int_{r_c}^{\infty}dr\int_{-r}^{r}d\Delta z\sum_{i=1}^{N_s}[\rho(z_{k+i})-\rho(z_{k+i-1})]rU_{\mathrm{LJ},m}(r), \tag{8}$$

where $\rho(z_k)$ and V_s are, respectively, the density and the volume of the slab k. Δz is defined as the difference $z-z_k$. N_s is the number of slabs between z and z_k. r_c is the cutoff radius, $U_{\mathrm{LJ},m}(r)$ is the intermolecular energy, and r is the distance between the two centers of mass,

$$U_{\mathrm{LJ},m}(r)=\sum_{a}^{N_i}\sum_{b}^{N_j}4\epsilon_{ab}\left[\left(\frac{\sigma_{ab}}{r}\right)^{12}-\left(\frac{\sigma_{ab}}{r}\right)^{6}\right]. \tag{9}$$

The first part of the long range contribution has an analytical form identical to the one associated with a homogeneous system but uses the local density $\rho(z_k)$ of the slab. The second part consists of a double integral which contains a series of density differences which render this part cumbersome to calculate. Concerning the second part of the LRCs to the total configurational energy, it has been shown[27,28] that it represents only a minor contribution to the total long range energy. The different contributions to the total energy are given in Table III for each system. The total energy calculated in an heterogeneous system must be only used for comparison between the different contributions and has no physi-

Downloaded 04 Jul 2008 to 194.214.132.32. Redistribution subject to AIP license or copyright; see http://jcp.aip.org/jcp/copyright.jsp

cal meaning due to the fact that its value is not constant throughout the z direction. The LRCs to the repulsion-dispersion energy (U_{LRC}) represent less than 1% of the total energy for water. This percentage increases up to 3% for H_2S and to 10% for n-alkanes. The electrostatic interactions are higher than the dispersion interactions in the case of water, whereas they are equal in magnitude to the dispersion interactions in the cases of CO_2 and H_2S. As a result, the thermodynamic properties calculated in the liquid-vapor interface of water should be little dependent on the calculation of the LRCs due to the truncation of the repulsion-dispersion interactions. By contrast, the use of appropriate LRCs due to the truncated potentials is required for the calculation of thermodynamic properties for CO_2 and H_2S. As expected from Table III, we will see throughout this paper that the LRC part to the surface tension of CO_2 and H_2S significantly contributes to the total surface tension.

B. Computational procedures

The simulation box is a rectangular parallelepipedic box of dimensions $L_xL_yL_z$ ($L_x=L_y$) with ($N=512$) H_2O, CO_2, or H_2S molecules. The details of the geometry of the system are given in Table II. The periodic boundary conditions were applied in the three directions. MC simulations were performed in the NVT ensemble. Each cycle consisted of N randomly selected moves with fixed probabilities. Two types of MC moves are performed with relative probabilities of 0.5 each: the translation of the center of mass of a random molecule and the rotation of a randomly selected molecule around its center of mass.

The initial configuration was built by placing N molecules on nodes of a fcc centered orthorombic lattice included in a cubic box. The nodes of the lattice were randomly chosen and the orientation of the molecules was random. MC simulations in the NpT ensemble were first performed on this bulk monophasic fluid configuration. The dimension of the resulting box was increased along the z axis by placing two empty cells on both sides of the bulk liquid box. A typical MC run consisted of 200 000 cycles for equilibration and 200 000 cycles for the production phase.

The thermodynamic properties were calculated every 10 cycles leading to the storage of 20 000 configurations. The statistical errors for these properties were estimated by using the jackknife method.[29] This method used four superblocks which are formed by combining three blocks of 5000 configurations. One of the specificity of our MC methodology was the use the LRCs to the configurational energy in the Metropolis scheme. The total LRC energy U_{LRC} was updated after each move of molecular position and is added in the total energy of the system to be used in the Metropolis scheme.

C. Surface tension

The most commonly used methods[30–35] for the surface tension calculation are based on the mechanical route definition and the use of tensorial components of the pressure. The first explicit form expresses the components of the pressure tensor as a function of the derivative of the intermolecular potential. This operational expression was given by Kirkwood and Buff[31] and is referred to as the KB expression (γ_{KB}). The definition of Irving and Kirkwood[32] (γ_{IK}) is based on the notion of the force across a unit area and takes advantage of expressing the local components of the pressure tensor along the direction normal to the surface. A novel method based on the thermodynamic definition of the surface tension (γ_{TA}) has been recently established by Gloor *et al.*[35] and consists of perturbing the cross-sectional area of the system containing the interface. We have also established a local version of the surface tension[36] (γ_{KBZ}) from the derivative of the potential with respect to the surface. In what follows, we present the different operational expressions of the surface tension with the corresponding expressions of their LRCs. Let us consider a system of N molecules with two planar liquid-vapor surface lying in the x,y plane.

1. Kirkwood–Buff relation

The molecular surface tension γ_{KB} was first introduced by Kirkwood and Buff[31] and makes use of the molecular virial expression to give the following relationship:

$$\gamma_{KB} = \frac{1}{2A}\left\langle \sum_{i=1}^{N-1}\sum_{j=i+1}^{N}\sum_{a=1}^{N_i}\sum_{b=1}^{N_j} \times \frac{\mathbf{r_{ij}}\cdot\mathbf{r_{iajb}} - 3z_{ij}\cdot z_{iajb}}{2r_{iajb}}\frac{dU(r_{iajb})}{dr_{iajb}}\right\rangle. \quad (10)$$

Specific LRCs have been developed by Blockhuis *et al.*[37] and are based on the approximations that the radial distribution function is equal to unity for r greater than the cutoff radius and that the density profile can be fitted to a hyperbolic function. This LRC expression takes the following form:

$$\gamma_{LRC} = \frac{\pi}{2}(\rho_l - \rho_v)^2 \int_0^1 ds \int_{r_c}^{+\infty} dr \coth\left(\frac{2rs}{d}\right)\frac{dU_{LJ,m}}{dr} \times r^4(3s^3 - s), \quad (11)$$

where d is an estimation of the thickness of the interface and s is a parameter defined as $s=(z_i-z_j)/r_{ij}$.

2. Irving–Kirkwood definition

By using the method of Irving and Kirkwood[32] for the expression of the local components of the pressure tensor, the surface tension becomes

$$\gamma_{IK} = \frac{1}{2}\int_{-L_z/2}^{L_z/2}(p_N(z_k) - p_T(z_k))dz, \quad (12)$$

where $p_N(z_k)$ and $p_T(z_k)$ are the normal and tangential components of the pressure tensor along the normal to the surface, respectively. The method of Irving and Kirkwood[32] is based on the notion of the force across a unit area. The pressure tensor is then written as a sum of a kinetic term and a potential term resulting from the intermolecular forces. Whereas the first term is well-defined, the potential term is

Downloaded 04 Jul 2008 to 194.214.132.32. Redistribution subject to AIP license or copyright; see http://jcp.aip.org/jcp/copyright.jsp

subjected to arbitrariness because there is no unique way to determine which intermolecular forces contribute to the stress across dA. There are many ways of choosing the contour joining two interacting particles. Irving and Kirkwood[32] have chosen as a contour the straight line between the two particles. Other choices are possible and result from the lack of uniqueness in the definition of the microscopic stress tensor. The components of the pressure[30,33,34] tensor in the Irving–Kirkwood (IK) definition are expressed as

$$p_{\alpha\beta}(z_k) = \langle \rho(z_k) \rangle k_B T \mathbf{I} + \frac{1}{A} \left\langle \sum_{i=1}^{N-1} \sum_{j>i}^{N} (\mathbf{r_{ij}})_\alpha (\mathbf{F_{ij}})_\beta \frac{1}{|z_{ij}|} \times \theta\left(\frac{z_k - z_i}{z_{ij}} \right) \theta\left(\frac{z_j - z_k}{z_{ij}} \right) \right\rangle, \tag{13}$$

where $\mathbf{I}$ is the unit tensor and T is the input temperature. α and β represent x, y, or z directions. $\theta(x)$ is the unit step function defined by $\theta(x)=0$ when $x<0$ and $\theta(x)=1$ when $x \geqslant 0$. A is the surface area normal to the z axis. The distance z_{ij} between two molecular centers of mass is divided into N_s slabs of thickness δz. Following the work of Irving and Kirkwood, the molecules i and j give a local contribution to the pressure tensor in a given slab if the line joining the centers of mass of molecules i and j crosses, starts or finishes in the slab. Each slab has $1/N_s$ of the total contribution from the i-j interaction. The normal component $p_N(z_k)$ is equal to $p_{zz}(z_k)$, whereas the tangential component is given by $\frac{1}{2}(p_{xx}(z_k) + p_{yy}(z_k))$. $\mathbf{F}_{ij}$ in Eq. (13) is the intermolecular force between molecules i and j and is expressed as the sum of all the site-site forces acting between these two molecules,

$$\mathbf{F_{ij}} = \sum_{a=1}^{N_i} \sum_{b=1}^{N_j} (\mathbf{f_{iajb}}) = - \sum_{a=1}^{N_i} \sum_{b=1}^{N_j} \frac{\mathbf{r_{iajb}}}{r_{iajb}} \frac{dU(r_{iajb})}{dr_{iajb}}. \tag{14}$$

The different contributions to be included in the calculation of the pressure components are given for completeness in the Appendix A in the case where the dispersion-repulsion and electrostatic interactions are calculated by using the LJ potential and Ewald summation technique, respectively.

The appropriate LRCs to the IK definition of the normal and tangential components of the pressure tensor have been derived by Guo and Lu[27] and are composed of two parts as expressed in Eqs. (15) and (16),

$$\begin{aligned} p_{N,\mathrm{LRC}}(z_k) &= p^{(1)}_{N,\mathrm{LRC}}(z_k) + p^{(2)}_{N,\mathrm{LRC}}(z_k) \\ &= -\frac{2\pi}{3} \rho^2(z_k) \int_{r_c}^{\infty} dr r^3 \frac{dU_{\mathrm{LJ},m}(r)}{dr} \\ &\quad - \pi \rho(z_k) \int_{r_c}^{\infty} dr \int_{-r}^{r} d\Delta z [\rho(z) \\ &\quad - \rho(z_k)] \frac{dU_{\mathrm{LJ},m}(r)}{dr} (\Delta z)^2. \end{aligned} \tag{15}$$

Concerning the tangential pressure, only the second term is modified and is expressed by Eq. (16),

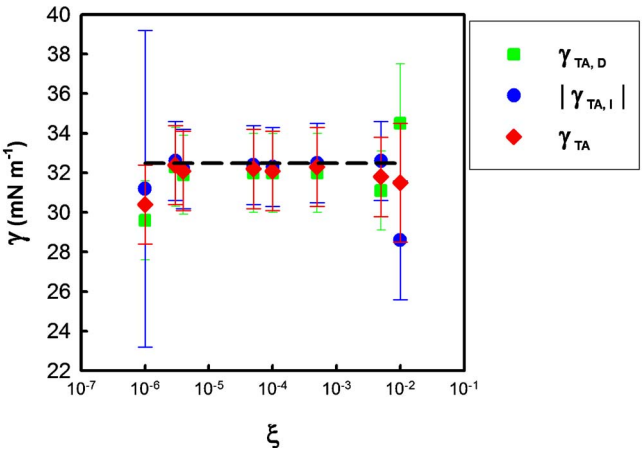

FIG. 1. (Color online) Direct $\gamma_{\mathrm{TA,D}}$, reverse $|\gamma_{\mathrm{TA,I}}|$, and average surface γ_{TA} tension values calculated from the test-area method for the liquid-vapor interface of CO_2 at $T=227$ K as a function of ξ. The dotted line corresponds to the average value of γ calculated from $\xi=5\times10^{-4}$.

$$p^{(2)}_{T,\mathrm{LRC}}(z_k) = -\frac{\pi}{2} \rho(z_k) \int_{r_c}^{\infty} dr \int_{-r}^{r} d\Delta z [\rho(z) - \rho(z_k)] \frac{dU_{\mathrm{LJ},m}(r)}{dr} [r^2 - (\Delta z)^2]. \tag{16}$$

The first term of $p_{N,\mathrm{LRC}}(z_k)$ and $p_{T,\mathrm{LRC}}(z_k)$ is identical to that used in homogeneous molecular simulations by using a local density $\rho(z_k)$ instead of a scalar density ρ, whereas the second term takes into account the density differences in the slabs. From these LRC expressions, it is then possible to calculate the LRC parts relative to the surface tension. The operational expression of the LRC part of the surface tension[27] within the IK formalism is then given by

$$\gamma_{\mathrm{LRC}}(z_k) = \frac{\pi}{2} \rho(z_k) \frac{V_s}{A} \int_{r_c}^{\infty} dr \int_{-r}^{r} d\Delta z \sum_{i=1}^{N_s} [\rho(z_{k+i}) - \rho(z_{k+i-1})] \frac{dU_{\mathrm{LJ},m}}{dr} [r^2 - 3(\Delta z)^2]. \tag{17}$$

The total LRC to the surface tension is obtained by summing up all the contributions to the local values of each bin and dividing the result by 2.

3. Test-area method

The recently developed test-area method[35] (TA) is based on a thermodynamic route and expresses the surface tension as a change in the free energy for an infinitesimal change in the surface area in the constant-NVT ensemble. This infinitesimal change in the area is performed throughout a perturbation process for which the perturbed system (state $A+\Delta A$) is obtained from an infinitesimal change ΔA in the area A. The box dimensions are then changed by a small quantity ξ such as $\xi \ll 1$. The box dimensions $(L_x^{(A+\Delta A)}, L_y^{(A+\Delta A)}, L_z^{(A+\Delta A)})$ in the perturbed systems are changed by using the following transformations: $L_x^{A+\Delta A} = L_x^{(A)}\sqrt{1+\xi}$, $L_y^{(A+\Delta A)} = L_y^{(A)}\sqrt{1+\xi}$, and $L_z^{(A+\Delta A)} = L_z^{(A)}/(1+\xi)$, where the superscript (A) refers to the

Downloaded 04 Jul 2008 to 194.214.132.32. Redistribution subject to AIP license or copyright; see http://jcp.aip.org/jcp/copyright.jsp

reference system. The area $(A+\Delta A)$ in the perturbed state is changed as $L_x^{(A)}L_y^{(A)}(1+\xi)$, where $\Delta A=L_x^{(A)}L_y^{(A)}\xi$. These transformations conserve the volume of the box in the perturbed state. This means that it is possible to express the surface tension as a ratio of partition functions between the perturbed and reference states. $U^{(A)}(\mathbf{r}^N)$ and $U^{(A+\Delta A)}(\mathbf{r}'^N)$ are the configurational energies of the systems with an area A and a configurational space $\mathbf{r}^N$ and an area $A+\Delta A$ and a configurational space $\mathbf{r}'^N$, respectively. The transformations used for the change in the volume lead to the following equality $d\mathbf{r}'^N=d\mathbf{r}^N$. This expression is the key for writing the surface tension as the average of $\exp(-\Delta U/kT)$ in the constant-NVT ensemble,

$$\gamma_{\mathrm{TA}}=\left(\frac{\partial F}{\partial A}\right)_{N,V,T}=\lim_{\xi\to 0}-\frac{k_BT}{\Delta A}\times\ln\left\langle\exp\left(-\frac{(U^{(A+\Delta A)}(\mathbf{r}'^N)-U^{(A)}(\mathbf{r}^N))}{k_BT}\right)\right\rangle_0=\sum_k\lim_{\xi\to 0}-\frac{k_BT}{\Delta A}\times\ln\left\langle\exp\left(-\frac{(U^{(A+\Delta A)}(z_k,\mathbf{r}'^N)-U^{(A)}(z_k,\mathbf{r}^N))}{k_BT}\right)\right\rangle_{k,A},\tag{18}$$

where $<\cdots>_{k,A}$ indicates that the average is carried out over the reference state and the k slabs. $U^{(A+\Delta A)}(z_k,\mathbf{r}'^N)$ and $U^{(A)}\times(z_k,\mathbf{r}^N)$ are the configurational energies of the slab k in the perturbed and reference states, respectively. The ambiguity[30] focuses on the part of the interaction energy to be included in the volume V_s of the slab. We adopt the definition of Ladd and Woodcok[38] and choose to assign in the slab centered on z_k two energy contributions: one contribution due to the energy between the molecules within the slab and a second contribution due to the energy of the molecules within the slab with those outside the slab. The energy of the slab at the position z_k is defined as

$$U_{z_k}=\frac{1}{2}\sum_{i=1}^{N}\sum_{j\neq i}^{N}\sum_{a}^{N_i}\sum_{b}^{N_j}H_k(z_i)U_{\mathrm{LJ}}(r_{iajb}),\tag{19}$$

where $H_k(z_i)$ is a top-hat function with functional values of

$$H_k(z_i)=1\quad\text{for } z_k-\frac{\delta z}{2}<z_i<z_k+\frac{\delta z}{2},$$

$$H_k(z_i)=0\quad\text{otherwise}.\tag{20}$$

By using this definition, we respect the following condition:

$$\int_V dz_k U_{z_k}=U,\tag{21}$$

where U is the total configurational energy of the simulation box and V its volume.

Concerning the LRC contributions to the surface tension calculated from the TA method, the total LRC contribution is expressed as a function of the total LRC energy U_{LRC} as in Eq. (22). We have already shown[14] that the difference between the $u_{\mathrm{LRC}}^{(1),(A+\Delta A)}(z_k')$ and $u_{\mathrm{LRC}}^{(1),(A)}(z_k)$ vanishes because the transformation conserves the volume. It results that the local LRC contribution to the TA approach is given by the second expression in Eq. (22). The total value of the tail correction of the surface tension within the TA formalism is expressed in Eq. (22),

$$\gamma_{\mathrm{LRC}}=\lim_{\xi\to 0}-\frac{k_BT}{\Delta A_\xi}\ln\left\langle\exp\left(-\frac{(U_{\mathrm{LRC}}^{(A+\Delta A)}-U_{\mathrm{LRC}}^{(A)})}{k_BT}\right)\right\rangle_0=\sum_k^{N_s}\lim_{\xi\to 0}-\frac{k_BT}{\Delta A_\xi}\times\ln\left\langle\exp\left(-\frac{(u_{\mathrm{LRC}}^{(2),(A+\Delta A)}(z_k'))-(u_{\mathrm{LRC}}^{(2),(A)}(z_k))}{k_BT}\right)\right\rangle_0=\sum_k^{N_s}\gamma_{\mathrm{LRC}}(z_k).\tag{22}$$

The calculation of the surface tension is carried out in the direct $(\gamma_{\mathrm{TA,D}})$ and reverse $(\gamma_{\mathrm{TA,I}})$ directions. The calculation of the direct direction involves an increase of the surface area $(A+\Delta A)$, whereas a decrease of the surface area $(A-\Delta A)$ is performed in the reverse path. Thermodynamic consistency requires that the surface tension in the direct and reverse directions must be equal in magnitude and in opposite sign. This is satisfied when the configuration space of the perturbed system matches to the one of the reference system. This requirement implies the use of an appropriate value of ξ. The value of ξ must satisfy two constraints:[35] this value should be small to allow an accurate calculation of the surface tension from Eq. (18) and large enough to provide reasonable statistics for the Boltzmann factor. The surface tension value is averaged over the two directions as $(\gamma_{\mathrm{TA,D}}-\gamma_{\mathrm{TA,I}})/2$. However, when the results differ between the two directions, there is no fundamental basis to justify that the errors cancel when averaging the direct and inverse values. One way to check the TA calculation is to compare the average surface tension with other values resulting from different approaches and to check the impact of the value of ξ on the calculation of the surface tension.

The influence of the value of ξ is illustrated in Fig. 1, where the values of the surface tension in the direct and reverse paths are reported as a function of ξ. Figure 1 shows that the absolute value of the surface tension in the reverse path matches very well that obtained in the forward direction for ξ ranging from 10^{-5} to 10^{-3}. The value $\xi=5\times10^{-4}$ used both in this work and in previous studies[20,35,39] is shown to be an appropriate value for the calculation of the surface tension by using the TA approach. The perturbation of the box dimensions is performed over the configurations of the reference state and leads to virtual configurations of the perturbed state. The ensemble average is carried out over the reference system, and the virtual configurations of the perturbed system do not participate to the Markov chain of states. We underline that the reciprocal space vectors change as the dimensions of the box are modified and must be recalculated after each virtual change of the surface area.

Downloaded 04 Jul 2008 to 194.214.132.32. Redistribution subject to AIP license or copyright; see http://jcp.aip.org/jcp/copyright.jsp

TABLE IV. Surface tension values (mN m^{-1}) of carbon dioxide at $T=238$ K calculated from MC simulations by using different box dimensions and number of molecules. The long range correction (LRC) contribution and the total surface tension are given for each method. The subscripts give the accuracy of the last decimal(s), i.e., 11.8_{10} means 11.8 ± 1.0. The experimental surface tensions (Ref. 46) (γ_{expt}) are reported for comparison.

	γ_{KB}		γ_{IK}		γ_{TA}		γ_{KBZ}		
T (K)	γ_{LRC}[a]	γ_{tot}[b]	γ_{LRC}[c]	γ_{tot}[d]	γ_{LRC}[e]	γ_{tot}[f]	γ_{LRC}[g]	γ_{tot}[h]	γ_{expt}
				$N=512$, $L_x=L_y=25.4$ Å, $L_z=150.8$ Å					
238	3.1_2	11.8_{10}	2.5_5	11.5_{10}	1.8_5	11.7_{10}	2.1_3	11.0_{10}	12.0
				$N=768$, $L_x=L_y=32.4$ Å, $L_z=150.8$ Å					
238	3.0_2	11.9_{10}	2.1_5	11.8_{10}	2.3_5	12.6_{10}	2.0_3	11.9_{10}	12.0
				$N=1024$, $L_x=L_y=25.4$ Å, $L_z=200.8$ Å					
238	3.5_2	12.1_{10}	2.2_5	11.5_{10}	2.1_5	11.8_{10}	1.9_3	11.9_{10}	12.0
				$N=1024$, $L_x=L_y=32.4$ Å, $L_z=200.8$ Å					
238	2.9_1	11.9_{10}	2.6_3	11.2_{10}	1.7_4	11.8_{10}	2.0_3	11.2_{10}	12.0

[a]Equation (11).
[b]Equations (11) and (10).
[c]Equation (17).
[d]Equations (17) and (12).
[e]Equation (22).
[f]Equations (22) and (18).
[g]Equation (24).
[h]Equations (24) and (23).

4. Local expression of the surface tension from the virial route (KBZ)

The original working expression of Kirkwood and Buff[31] does not provide a profile of the surface tension as a function of the direction normal to the interface. The profile becomes a key element from a methodological viewpoint to check the validity of the calculation concerning the stabilization of the interfaces, the independence between the two interface, and the constancy of the pseudolocal surface tension $\gamma(z)$ in the bulk regions. We have then established a local version[36] of the surface tension based on the KB expression (KBZ). The working expression has been obtained from the derivative of the potential with the respect to the surface and is referred as the KBZ method in this paper.

$$\gamma_{KBZ} = \left\langle \frac{\partial U}{\partial A} \right\rangle_0 = \sum_k^{N_s} \left\langle \frac{\partial U_{z_k}}{\partial A} \right\rangle_0 . \tag{23}$$

We give for completeness the operational expression of γ derived from the KBZ approach in Appendix B. Additionally, we see that the operational expressions derived from the IK definition and the KBZ approach are equivalent even if these expressions are obtained from two different routes. We have also a typical operational expression for the LRC contribution within the KBZ approach. The working local LRC expression has been established previously[36] and is then given by the following equation:

$$\gamma_{LRC}(z_k) = \pi\rho(z_k)\frac{V_s}{2A}\int_{r_c}^{\infty} dr \int_{-r}^{r} d\Delta z[\rho(z) - \rho(z_k)] \times \left(\frac{r^2 - 3(\Delta z)^2}{r}\right)\left(U_{LJ,m}(r) + r\frac{\partial U_{LJ,m}(r)}{\partial r}\right). \tag{24}$$

III. RESULTS AND DISCUSSIONS

A. Size effects

The calculation of the surface tension from the simulation of two-phase systems can be affected by the use of both periodic boundary conditions and small surface areas.[39,40] These recent works establish an oscillatory function of the intrinsic part of the surface tension of LJ fluids for small surface areas and a constant value of the surface tension with larger surface areas. Beyond an interfacial area of $(7\times7\sigma^2)$, where σ is the diameter of the LJ particle, we observe that the maximum variation in the intrinsic part of the surface tension does not exceed 15% of the constant value of γ. The interfacial area used in this work approximately corresponds to the value of $(7\times7\sigma^2)$. Let us recall that we must maintain an objective of computational efficiency for the two-phase simulation with respect to the simulation carried out with the Gibbs ensemble MC methods.[41] As a result, we aim to find a compromise between the system size and the CPU time. We evaluate then the impact of the box dimensions on the calculation of the surface tension by keeping the surface area constant and changing the L_z dimension and vice versa. Direct MC simulations were then performed for $N=512$, 768, and 1024 system sizes for the liquid-vapor interface of CO_2 at $T=238$ K. The different contributions to the surface tensions are given in Table IV for the KB, IK, TA, and KBZ approaches. We do not observe a trend of the surface tension over this range of system sizes. The results show that the total surface tension is little dependent on the system size due to the fact that the changes in the surface tension are within the fluctuations estimated by using the variation in the block averages. Additionally, these variations in the surface tension are comparable to those induced by the calculation of γ by using different definitions. The magnitude of the fluctuations of the surface tension can be attributed to the fact that we are simulating molecular systems interacting through dispersion-repulsion and electrostatic interactions by contrast to those obtained in the simulation of LJ fluids. These fluctuations are of the same order of magnitude as those induced by the dependence of the surface tension with the surface area beyond an area of $(7\times7\sigma^2)$. The fact that the surface tension remains unchanged within the statistical fluctuations when increasing the system size has already been observed

Downloaded 04 Jul 2008 to 194.214.132.32. Redistribution subject to AIP license or copyright; see http://jcp.aip.org/jcp/copyright.jsp

TABLE V. Surface tension values (mN m^{-1}) of water calculated from MC simulations by using different operational expressions. The long range correction (LRC) contribution and the total surface tension are given for each method. The subscripts give the accuracy of the last decimal(s), i.e., 63.7_{30} means 63.7 ± 3.0. The experimental surface tensions (Ref. 46) (γ_{expt}) are reported for comparison.

	γ_{KB}		γ_{IK}		γ_{TA}		γ_{KBZ}		
T (K)	γ_{LRC} [a]	γ_{tot} [b]	γ_{LRC} [c]	γ_{tot} [d]	γ_{LRC} [e]	γ_{tot} [f]	γ_{LRC} [g]	γ_{tot} [h]	γ_{expt}
					Water, TIP4P/2005				
298	4.6_1	70.8_{40}	6.1_1	72.3_{40}	4.1_2	71.8_{40}	5.1_1	71.2_{40}	71.9
328	4.4_2	65.6_{40}	5.9_1	67.1_{40}	3.9_2	66.8_{40}	4.9_1	65.9_{30}	67.1
358	4.2_2	62.4_{30}	5.5_1	63.7_{30}	3.8_2	64.1_{30}	4.6_1	64.6_{30}	61.7
388	4.0_1	55.8_{40}	5.2_1	57.0_{40}	3.5_2	55.5_{40}	4.3_1	56.1_{40}	55.9
418	3.7_1	49.7_{20}	4.9_1	50.7_{20}	3.4_2	51.0_{30}	4.1_1	51.5_{20}	49.8
448	3.4_2	40.8_{30}	4.4_1	41.8_{30}	3.0_2	42.1_{30}	3.7_1	42.6_{20}	43.3
478	3.1_2	33.2_{40}	3.5_1	33.6_{40}	2.5_2	34.0_{40}	3.0_1	34.2_{40}	36.5
508	2.8_1	32.2_{30}	2.8_1	32.2_{30}	2.3_2	32.5_{30}	2.4_1	32.7_{30}	29.5
538	2.3_1	24.9_{20}	2.2_1	24.7_{20}	1.6_2	25.0_{30}	1.9_1	25.1_{20}	22.5
568	2.1_1	13.4_{20}	2.1_1	13.4_{20}	1.5_2	12.4_{20}	1.7_1	12.7_{20}	15.5
598	1.7_1	8.6_{10}	2.0_1	8.9_{10}	1.4_2	8.8_{30}	1.7_1	8.2_{30}	8.8

[a]Equation (11).
[b]Equations (11) and (10).
[c]Equation (17).
[d]Equations (17) and (12).
[e]Equation (22).
[f]Equations (22) and (18).
[g]Equation (24).
[h]Equations (24) and (23).

for the calculation of the surface tension of water.[16] It was also established by Guo and Lu[27] that taking into account the LRC contributions to the configurational energy in the Metropolis scheme allows us to obtain reliable surface tensions with a smaller total number of molecules. We have also underlined this point in the case of a previous work[28] dealing with the calculation of surface tensions of *n*-alkanes.

B. Comparison with the experiments

Let us begin the discussions by the results of the surface tension of water. This calculation represents a prerequisite for the future study of the water-H_2S and water-CO_2 systems. A brief scan of the literature shows that there are a certain number of very recent papers[18,20,42–44] dealing with the surface tension calculation of water. Some of them[18,20,42,44] use the traditional rigid nonpolarizable models with the MD technique.[18,20,42,44] It has recently been established from MD calculations that the new reparametrization (TIP4P/2005) (Ref. 19) of the four-point TIP4P model[45] led to a good reproduction of the surface tension[20] over the whole range of temperatures from the triple point to the critical temperature. This representation of the water molecule (Table I) consists of four interaction sites: three of them are placed at the oxygen and hydrogen atom positions, whereas the fourth site is placed on the bisector of the H–O–H angle. It is then of fundamental interest to underline that the optimized parameters of the TIP4P/2005 model have been obtained from MC simulations by using a truncated potential and that the values of surface tension using this model have been calculated from MD simulations by using a potential modified by a switching function. These problems associated with the truncation of the potential were shown to be important in the case of simulations of two-phase systems where the LJ interactions were predominant. In the case of systems involving electrostatic interactions that are several orders of magnitude higher than the repulsion-dispersion energy contributions, the effects due to the truncation of the LJ potential should be significantly weakened. Given that our methodology uses the MC method, it is then essential to check the accuracy of the surface tension calculation from MC simulations by using the TIP4P/2005 model with a truncated potential.

Table V shows the LRCs and total contributions of the surface tension of water calculated from the KB, IK, TA, and KBZ techniques. We firstly observe that the values of the surface tension are independent of the method used once the LRC contributions are included in the calculation. We check that the calculated surface tensions are in excellent agreement with the experimental values[46] with a maximum deviation of 13%. Figure 2 compares the surface tensions calculated from our MC simulation using the IK definition with those resulting from previous MD calculations.[20] Interestingly, we observe that the calculated values of γ match very well within the statistical fluctuations suggesting that the truncation procedures used in MC and MD do not affect the results when electrostatic interactions are involved. The discussion of the different contributions to the surface tensions will be analyzed in the methodological part of this paper. Part (b) of Fig. 2 shows the phase envelope of water calculated from MC simulations and that resulting from the recent work of Vega *et al.*[20] The coexisting densities result from the fit to the molecular density profiles by using Eq. (25),

$$\rho(z_k) = \frac{1}{2}(\rho_l + \rho_v) - \frac{1}{2}(\rho_l - \rho_v)\tanh\left(\frac{2(z_k - z_0)}{d}\right), \qquad (25)$$

where ρ_l and ρ_v are the coexisting densities of the liquid and vapor phases, respectively. z_0 indicates the position of the Gibbs surface, and d represents the interfacial thickness. The coexisting densities calculated from MC simulations are in line with those calculated from MD simulations[20] and

Downloaded 04 Jul 2008 to 194.214.132.32. Redistribution subject to AIP license or copyright; see http://jcp.aip.org/jcp/copyright.jsp

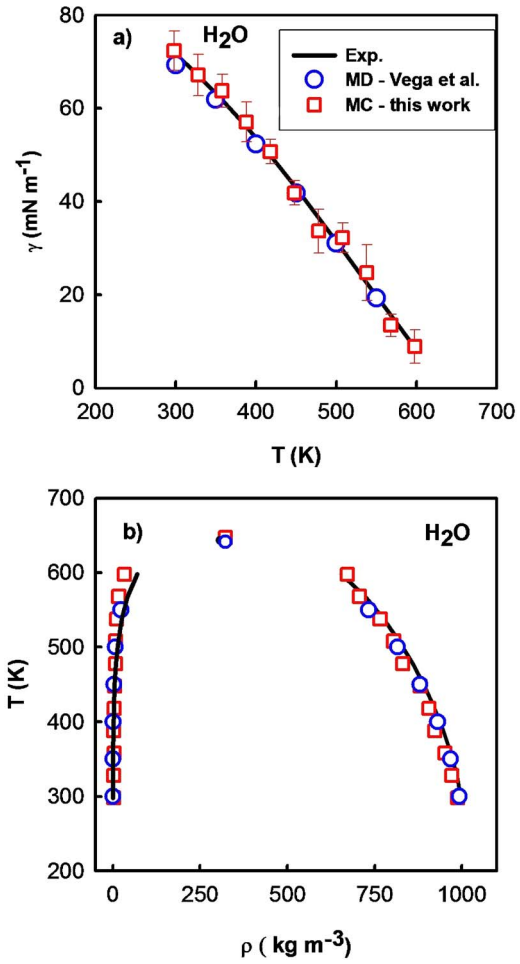

FIG. 2. (Color online) (a) Surface tension values calculated from the IK definition and (b) vapor-liquid coexistence density curve of water calculated from MC simulations (open squares) and previous MD simulations (open circles) by using the TIP4P/2005 model. The continuous lines represent the experimental values (Ref. 46).

experiments. The estimate of the critical point has been carried out by fitting the calculated coexistence density to the scaling law for the density and law of rectilinear diameters by using an Ising-type critical exponent of $\beta=0.32$. The calculated critical temperature (T_c) is equal to 641 K compared to an experimental value of 647 K. The critical densities (ρ_c) are 307 kg m^{-3} for MC and 322 kg m^{-3} for experiments. T_c is predicted within 1% by using MC, whereas ρ_c is predicted within 6%. These results confirm that the data provided from our methodology agree very well with the experiments and with the recent works of Vega *et al.* and establish the TIP4P/2005 water model as a very promising model for the simulation of two-phase system by using both MC and MD methods.

CO_2 is simulated by using the rigid version of the EPM2 intermolecular potential of Harris and Yung.[21] Carbon dioxide is described by a three site model (Table VI): one LJ sphere per atom and one point charge per atom. The results of the surface tension are given in Table VI and are represented in Fig. 3(a) as a function of the temperature. Table VI shows that the agreement between calculated and experimental surface tensions is excellent with deviations smaller than 10% up to 288 K. We also confirm that the different definitions of the surface tension give consistent values demonstrating then the correctness of the procedure used. The critical temperature calculated from the coexisting densities is 306 K and the critical density is 448 kg m^{-3}. We observe deviations of 4% and less than 1% with respect to the experiments for the critical temperature and density, respectively. We also report for completeness the liquid-vapor coexisting curve[47] calculated from Gibbs ensemble MC (GEMC) (Ref. 41) method. The comparison with the GEMC method confirms that the direct two-phase method also predicts very well the phase envelope of CO_2.

For H_2S, we have used the potential proposed by Kristof and Liszi[22] which involves a single LJ 6-12 site and four electrostatic point charges (see Table I). Figure 4(b) shows that the direct MC simulations are capable to correctly reproduce the coexisting densities of H_2S. The predicted phase

TABLE VI. Surface tension values (mN m^{-1}) of carbon dioxide calculated from MC simulations by using different operational expressions. The long range correction (LRC) contribution and the total surface tension are given for each method. The subscripts give the accuracy of the last decimal(s), i.e., 10.4_9 means 10.4 ± 0.9. The experimental surface tensions (Ref. 46) (γ_{expt}) are reported for comparison.

	γ_{KB}		γ_{IK}		γ_{TA}		γ_{KBZ}		
T (K)	γ_{LRC}[a]	γ_{tot}[b]	γ_{LRC}[c]	γ_{tot}[d]	γ_{LRC}[e]	γ_{tot}[f]	γ_{LRC}[g]	γ_{tot}[h]	γ_{expt}
				CO_2					
228	3.3_2	15.4_{20}	3.0_5	15.1_{20}	2.1_1	15.5_{20}	2.5_1	14.5_{20}	14.3
238	3.1_2	11.8_{10}	2.5_5	11.5_{10}	1.8_5	11.7_{10}	2.1_3	11.0_{10}	12.0
248	2.4_2	11.3_9	2.2_5	10.8_9	1.5_6	11.2_{10}	1.8_2	10.4_9	9.7
258	2.1_1	8.4_9	1.9_5	8.2_9	1.4_4	8.5_{10}	1.6_4	7.9_9	7.6
268	1.7_2	5.6_9	1.5_5	5.3_9	1.1_8	5.6_{10}	1.2_3	5.1_9	5.5
278	1.4_1	3.8_5	1.1_5	3.5_5	0.7_8	3.7_5	0.9_1	3.3_5	3.6
288	0.9_1	2.7_6	0.8_5	2.6_6	0.6_9	2.8_6	0.6_4	2.5_6	2.0
298	0.8_2	1.0_1	0.4_5	0.7_1	0.3_5	0.8_2	0.4_2	0.6_1	0.6

[a]Equation (11).
[b]Equations (11) and (10).
[c]Equation (17).
[d]Equations (17) and (12).
[e]Equation (22).
[f]Equations (22) and (18)
[g]Equation (24).
[h]Equations (24) and (23).

Downloaded 04 Jul 2008 to 194.214.132.32. Redistribution subject to AIP license or copyright; see http://jcp.aip.org/jcp/copyright.jsp

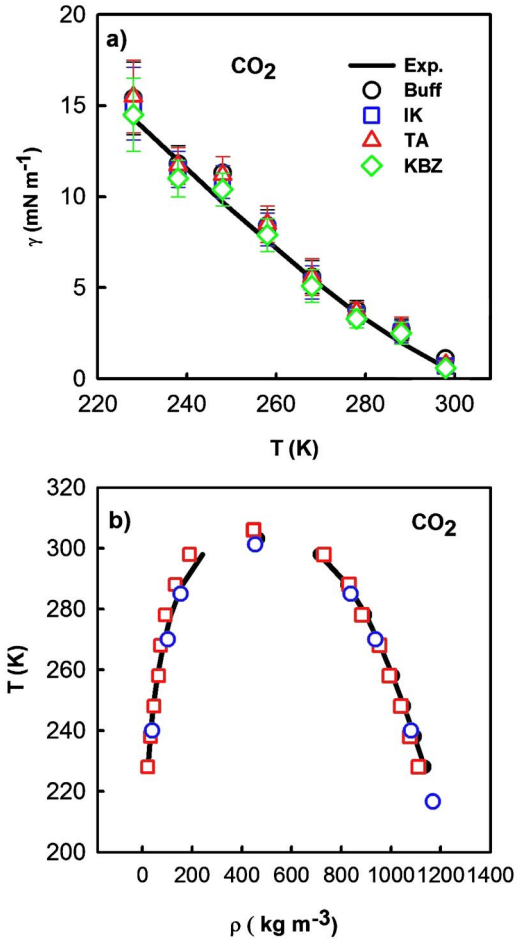

FIG. 3. (Color online) (a) Surface tension values of the liquid-vapor interface of carbon dioxide calculated from different methods, KB (open circles), IK (open squares), TA (open triangles), KBZ (open diamonds), and experimental values (solid line) (Ref. 46). (b) Vapor-coexistence curve of CO_2 calculated from MC simulations (open circles) and from GEMC (Ref. 47) (open squares). The continuous lines represent the experimental coexisting densities (Ref. 46).

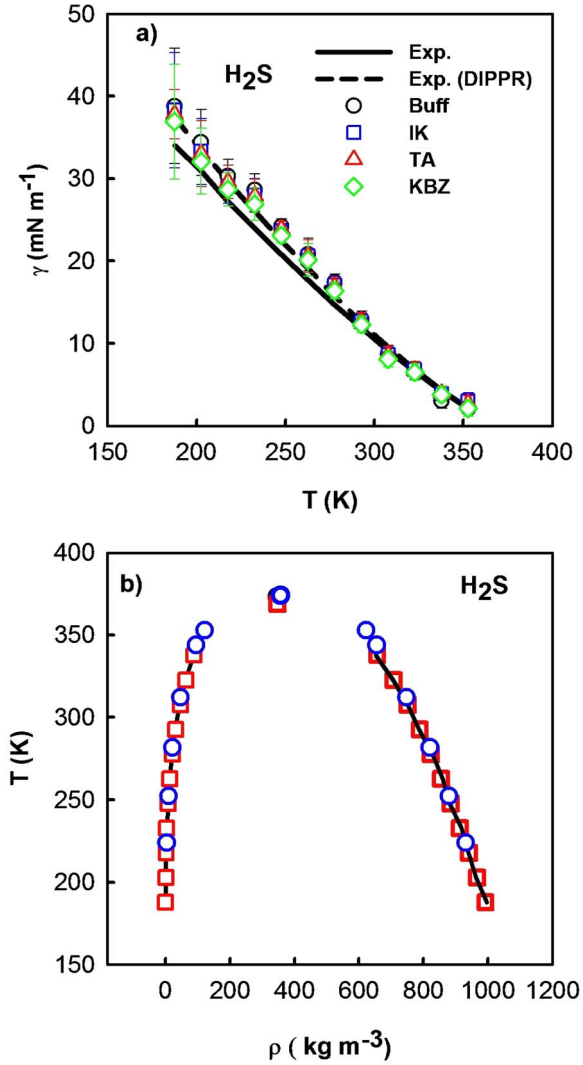

FIG. 4. (Color online) (a) Surface tension values of the liquid-vapor interface of hydrogen sulfide calculated from different methods, KB (open circles), IK (open squares), TA (open triangles), KBZ (open diamonds), experimental values (solid line), (Ref. 46) DIPPR correlations (dashed line). (b) Vapor-coexistence curve of and H_2S calculated from MC simulations (open circles) and from GEMC (Ref. 22) (open squares). The continuous lines represent the experimental coexisting densities (Ref. 46).

envelope is found to be in good agreement with that calculated from the original work of Kristof and Liszi[22] by using the GEMC method. The critical temperatures resulting from the liquid-vapor coexistence curve are equal to 369 K (MC), 374 K (GEMC),[22] and 373 K (experiments),[46] whereas the critical density is 347, 356 (GEMC),[22] and 347 kg m^{-3} (experiments).[46] The comparison between the critical properties coming from both experiments and simulations is very acceptable. Additionally, the calculated surface tension values reported in Table VII agree very well with the available experimental surface tensions and those derived from the DIPPR databank correlations.[48] Figure 4(a) confirms this viewpoint by showing that the surface tensions computed from the different routes are in line with the reference values coming from experiments and DIPPR databank correlations.[48]

It may be concluded that the coexisting liquid-vapor properties of pure water, carbon dioxide, and hydrogen sulfide are represented with a very good accuracy by using the MC two-phase simulation method. It also results from this study that the models used for H_2O, CO_2, and H_2S can be used with confidence for the prediction of the surface tension of pure systems. This is a result of primary importance for the forthcoming work consisting in calculating the interfacial tensions of binary mixtures such as water CO_2 and water H_2S. Typical configurations of the H_2S liquid-vapor interfaces are shown in Fig. 5 at two different temperatures.

The next section aims to check the validity and consistency of the procedure used for the simulation of a two-phase system when electrostatic interactions are computed. We already checked the mechanical, thermal, and chemical equilibria of two-phase simulations of *n*-alkanes.[14,15,28] However, the account of the electrostatic contributions, handled by using the Ewald method, requires us to check the validity of the different expressions of the surface tension through local calculations, to calculate the configurational temperature within the Ewald methodology and to carefully analyze the different contributions coming from LJ and Coulombic interactions in the surface tension.

Downloaded 04 Jul 2008 to 194.214.132.32. Redistribution subject to AIP license or copyright; see http://jcp.aip.org/jcp/copyright.jsp

TABLE VII. Surface tension values (mN m^{-1}) of hydrogen sulfide calculated from MC simulations by using different operational expressions. The long range correction (LRC) contribution and the total surface tension are given for each method. The subscripts give the accuracy of the last decimal(s), i.e., 38.3_{30} means 38.3 ± 3.0. The experimental surface tensions (Ref. 46) (γ_{expt}) are reported for comparison with those of the DIPPR databank correlations (Ref. 48).

	γ_{KB}		γ_{IK}		γ_{TA}		γ_{KBZ}		
T (K)	γ_{LRC} [a]	γ_{tot} [b]	γ_{LRC} [c]	γ_{tot} [d]	γ_{LRC} [e]	γ_{tot} [f]	γ_{LRC} [g]	γ_{tot} [h]	γ_{expt}, γ_{DIPPR}
					H_2S				
187	8.5_8	38.8_5	8.0_3	38.3_{30}	5.3_2	37.8_{30}	6.7_3	37.1_{30}	[34.0,37.5]
202	7.9_9	34.4_7	7.0_6	33.3_8	4.8_2	33.0_5	5.9_5	28.7_5	[31.0,33.5]
217	7.4_9	30.3_7	7.0_6	29.0_8	4.8_2	29.6_5	5.9_5	28.7_5	[27.2,29.7]
232	6.8_3	28.6_5	6.0_7	28.0_5	4.1_2	27.9_5	4.9_5	27.0_5	[24.0,26.1]
247	6.1_9	24.2_7	5.5_8	23.6_5	3.8_1	23.8_5	4.6_9	23.1_7	[20.8,22.5]
262	5.2_9	20.8_6	5.0_2	20.6_5	3.4_2	20.6_5	4.2_2	20.1_5	[17.7,19.1]
277	4.7_1	17.4_5	4.4_9	17.1_5	3.1_2	16.9_6	3.6_7	16.3_6	[14.7,15.7]
292	3.7_1	12.9_5	3.4_9	12.6_5	2.3_2	12.7_5	2.8_1	12.3_7	[11.9,12.5]
307	2.7_1	8.7_5	2.7_1	8.6_{10}	2.0_2	8.6_5	2.3_1	8.1_5	[9.1,9.5]
322	1.9_1	6.6_5	2.2_6	6.8_{10}	1.5_2	6.7_5	1.8_6	6.5_6	[6.6,6.8]
337	0.4_8	3.0_5	1.3_1	3.9_5	0.9_2	3.8_6	1.1_6	3.8_5	[4.2,4.3]
352	0.0_1	2.1_4	0.9_3	3.0_5	0.6_1	2.8_6	0.7_3	2.1_5	[2.1]

[a]Equation (11).
[b]Equations (11) and (10).
[c]Equation (17).
[d]Equations (17) and (12).
[e]Equation (22).
[f]Equations (22) and (18).
[g]Equation (24).
[h]Equations (24) and (23).

C. Methodological discussion

In the case of a planar liquid-vapor surface lying in the x,y plane, the density gradient takes place in the z direction normal to the interface. It is also of basic interest to check the bahavior of some local thermodynamic properties along this direction. Expressing the surface tension as a function of z is a key element to check the validity of the calculation concerning the stabilization of the interfaces, the independence between the two interfaces, and the constancy of $\gamma(z)$ in the bulk phases. It follows from this that the system is well equilibrated and that the contribution from the two surfaces is the same. It was demonstrated[36] that monitoring the accumulated average value of the surface tension as a function of the number of cycles was not always valid and it became meaningful to assess the profile of the surface tension to check the formation of two stable interfaces. Until recently, only the method of Irving and Kirkwood was designed to provide a profile of the surface tension along the direction normal to the interface. We established the local version of the surface tension by using the TA (Ref. 14) approach and KB (Ref. 36) method.

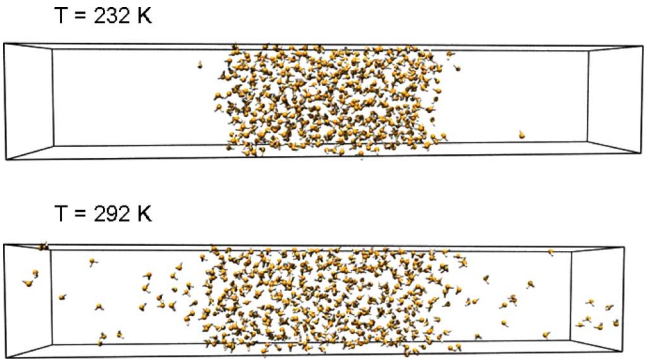

FIG. 5. (Color online) Configurations of hydrogen sulfide liquid-vapor interface at 232 and 292 K. Sulfur atoms are represented in yellow, while hydrogen atoms are in white.

Figure 6(a) shows the different profiles of the local intrinsic surface tension of CO_2 at $T=228$ K calculated from the IK, TA, and KBZ approaches by using Eqs. (12), (18), and (23), respectively. Interestingly, we observe from a methodological viewpoint that the profiles are symmetric and there are no contributions in the bulk phases. We also note that the different profiles match very well and that the resulting integral of Fig. 6(b) converges to similar values of surface tension. We also see, in Fig. 6(a), that the value of the surface tension calculated from the TA technique is a little higher than those of the two other methods based on the mechanical route. However, we check in Fig. 6(c) that the profiles of the LRC part of the surface tension calculated from the TA method present two peaks with the smallest amplitude. It means that the LRC contribution to the surface tension coming from the TA technique is smaller than those calculated by using IK and KBZ (see Table VI). This explains why the total value of the surface tension can be considered as identical within the statistical fluctuations between the IK, TA, and KBZ techniques. Additionally, we check that the total surface tension calculated from the integral of the local values is strictly identical to the surface tension calculated from the macroscopic expression indicating that the decomposition of the surface tension into local expressions is valid and consistent.

Part (a) of Fig. 7 shows that the molecular profiles for water and carbon dioxide contain two well-defined interfaces. We observe regions of bulk liquid of approximately 40 Å for both components which are considered as enough to make an accurate estimate of the liquid density. The density profiles are also symmetric around the middle of the slab. The fitted density profiles resulting from Eq. (25) are shown in a solid line to establish that they match very well with the average density along the z direction. This is an additional evidence that the direct simulation method is capable to produce reliable bulk coexisting densities calculated

Downloaded 04 Jul 2008 to 194.214.132.32. Redistribution subject to AIP license or copyright; see http://jcp.aip.org/jcp/copyright.jsp

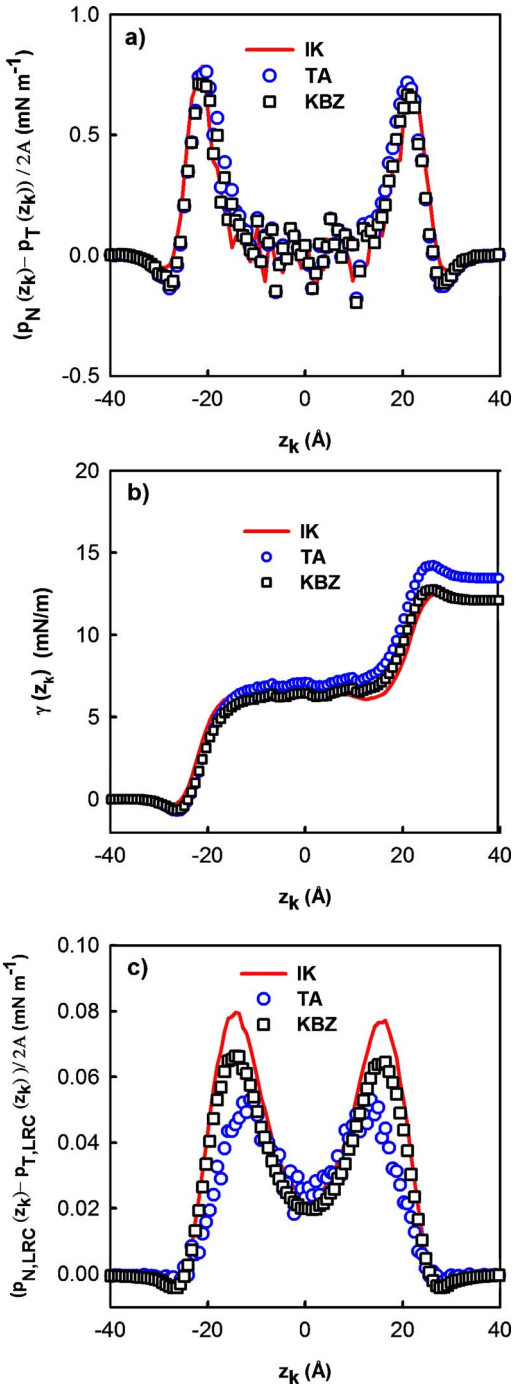

FIG. 6. (Color online) (a) $p_N(z_k)-p_T(z_k)$ for the sum of the Lennard-Jones and electrostatic contributions as a function of z_k at $T=228$ K for the liquid-vapor interface of CO_2 by using three different definitions. (b) Integral of $p_N(z_k)-p_T(z_k)$ as a function of z_k. (c) Profiles of $p_{N,LRC}(z_k)-p_{T,LRC}$ calculated by using the IK, TA, and KBZ approaches.

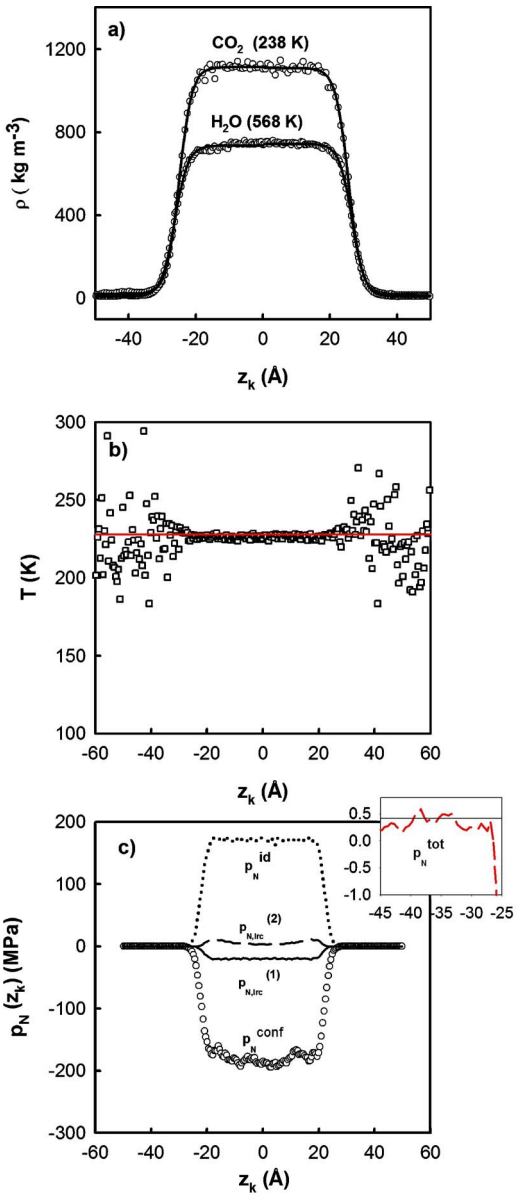

FIG. 7. (Color online) (a) Molecular density profiles for CO_2 and water (open circles). The solid lines are for the fitted tangent hyperbolic function. (b) Profile of the configurational temperature (open squares) for CO_2 at 228 K. The solid line corresponds to the Boltzmann temperature of 228 K. (c) Profiles of the different contributions of the normal component of the pressure tensor for water at 418 K. The inset shows the total normal component (dashed line) in the vapor phase, whereas the solid line correspond to the experimental vapor pressure in MPa.

from the fitted curves with densities corresponding to the experimental values [see Figs. 2(b), 3(b), and 4(b)].

We have already shown in previous papers[18,14,28] that the calculated configurational temperature from direct MC simulations matched very well with the Boltzmann temperature. This check was performed on the liquid-vapor interface of *n*-alkanes for which the modeling did not involve any electrostatic interactions. In the case of the calculation of Coulombic interactions handled with the Ewald method, it is essential to recover that the local configuration temperature along the direction normal to the interface agrees with the input temperature. To do so, we calculate the local configurational temperature from the following expression:

$$k_B T_{\mathrm{conf}}(z_k) = \frac{\left\langle \sum_{i=1, i\in k}^{N} \mathbf{F_i}^2 \right\rangle}{\left\langle -\sum_{i=1, i\in k}^{N} \left(\frac{\partial F_{ix}}{\partial r_{ix}} + \frac{\partial F_{iy}}{\partial r_{iy}} + \frac{\partial F_{iz}}{\partial r_{iz}} \right) \right\rangle}, \tag{26}$$

where i refers to the molecule and $\mathbf{F_i}=\Sigma_{j\neq i}^{N}\mathbf{F_{ij}}$. The calculation of the forces and of the derivatives with respect to the position vector are carried out by taking into account the contributions of the LJ potential and of the Ewald summation

Downloaded 04 Jul 2008 to 194.214.132.32. Redistribution subject to AIP license or copyright; see http://jcp.aip.org/jcp/copyright.jsp

TABLE VIII. Contributions of surface tensions (mN m^{-1}) derived from the Lennard-Jones contribution (γ^{LJ}), the real part (γ^{R}), and the two terms ($\gamma^{K,1}$, $\gamma^{K,2}$) of the reciprocal space part of the Ewald contribution. The expressions of these different terms are given through the components of the pressure tensor in Appendix A. The LRC term (γ_{LRC}) and the total term (γ_{tot}) calculated from the sum of the previous contributions are also reported.

γ^{LJ}	γ^{R}	$\gamma^{K,1}$	$\gamma^{K,2}$	γ_{LRC}	γ_{tot}
		Water, TIP4P/2005 (T=478 K)			
−87.6	112.1	−6.4	12.0	3.5	33.6
		CO_2 (T=238 K)			
6.1	2.0	−0.8	1.7	2.5	11.5
		H_2S (T=187 K)			
21.0	8.0	−1.5	2.8	8.0	38.3

technique. Further details about the definition of the configurational temperature can be found elsewhere.[49–52] The local thermal equilibrium can be demonstrated from MC simulations by calculating the local configurational temperature. Figure 7(b) shows a profile of $T_{conf}(z_k)$ for the simulation of CO_2 at T=228 K. We observe that the local temperature in the liquid and vapor regions matches very well with the Boltzmann temperature. The average temperature calculated over the slabs in the liquid region is 227 ± 2 K, whereas it is equal to 225 ± 20 K in the vapor phases. The increase of the standard deviation in the vapor phases is essentially attributed to the statistics resulting from a smaller number of molecules. This calculation allows us to diagnose the correctness of the procedure used for the simulation of a two-phase system with electrostatic interactions by using a MC method.

Figure 7(c) aims to show the different contributions of the normal component of the pressure tensor in the case of the liquid-vapor interface of water at T=418 K. We separate the pressure of Eq. (13) into the ideal gas contribution and the potential part. We also show the profiles of the two contributions of the LECs to the pressure given in Eq. (15). Interestingly, we observe that the profile of the LRCs of the normal pressure only represent 10% of either the ideal gas contribution or the configurational contribution. It was not the case in the simulation of the liquid-vapor interface of *n*-alkanes where the LRC parts to the normal pressure were in the same order of magnitude as the ideal and configurational parts. This is due to the introduction of electrostatic interactions in the model. We also check that the profile of the total normal pressure, plotted as an inset of Fig. 7(c), fluctuates in the vapor phase around an average value in agreement with the experimental vapor pressure (0.41 MPa at 418 K from DIPPR correlations[48]).

It is also of fundamental interest to compare the different contributions to the surface tensions in the water, carbon dioxide, and hydrogen sulfide systems. The different contributions are given for comparison in Table VIII. The working expressions of these contributions are given through the components of the pressure tensor in Appendix A. Firstly, we check that the magnitude and the sign of the different contributions given for the water system are in agreement with those given in the work of Alejandre *et al.*[15] The slight differences between the values are due to the model used for water and the temperature. Concerning the liquid-vapor interface of water, we observe a negative contribution to γ from the LJ part. As expected, Fig. 8(a) allows us to check that these negative contributions come from the interfacial region. The sign of this contribution could be explained by the fact that the oxygen-oxygen distance is smaller than the value of σ in the interfacial region leading to positive values of the LJ potential (see Table I). The decrease in the oxygen-oxygen distance could be explained by stronger electrostatic interactions. This was already observed in a study of Rivera *et al.*[43] We also check that the LRC contribution to γ is relatively weak compared to that calculated in *n*-alkanes systems governed only by dispersion-repulsion interactions.

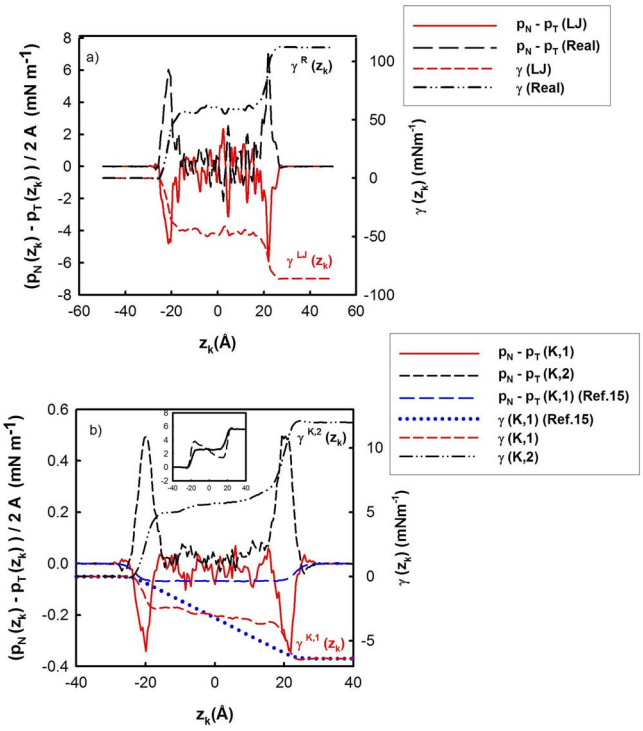

FIG. 8. (Color online) (a) $p_N(z_k) - p_T(z_k)$ for the Lennard-Jones and for the real part of the potential as a function of z_k for water at 478 K. The dashes lines correspond to the integral of $p_N(z_k) - p_T(z_k)$ as a function of z_k (right axis) as indicated in the legend. (b) $p_N(z_k) - p_T(z_k)$ profiles of the two contributions of the reciprocal part of the potential with their corresponding integral curves (dashed curves). The inset shows the integral of the $p_N(z_k) - p_T(z_k)$ profile of the reciprocal space part of the potential as a function of z_k by using two different definitions, this work (solid line) and the work of Alejandre *et al.* (Ref. 15) (dashed line).

Downloaded 04 Jul 2008 to 194.214.132.32. Redistribution subject to AIP license or copyright; see http://jcp.aip.org/jcp/copyright.jsp

This is in line with the previous observations made on the value of the tail corrections to the normal pressure. In the case of H_2S which is slightly less polar than H_2O and weakly associated system, we find a positive value of the dispersion-repulsion contribution and a smaller real space contribution. We also observe a decrease in the real space contribution in the case of the quadrupolar CO_2 system.

Let us focus on the profiles of these different contributions in the case of water at 478 K. Part (a) of Fig. 8 presents the profiles of the dispersion-repulsion and real space contributions as a function of z. We observe that the integrals of these profiles are flat in the bulk regions indicating that only the two interface regions contribute to the total value of each contribution. Figure 8(b) shows the profiles of the first reciprocal $\gamma^{K,1}(z_k)$ term and second reciprocal $\gamma^{K,2}(z_k)$ term with their corresponding integral profiles represented on the right axis. The profile of the working expression of $\gamma^{K,1}(z_k)$ given in Eq. (A4) is calculated by summing all the contributions of each molecule whose center of mass belongs to the z slab. We adopt the same definition for the second term $\gamma^{K,2}(z_k)$. Concerning the first term, Alejandre *et al.* chose a different way of calculating this term. They assume that the contribution of this term to the surface tension $\gamma^{K,1}(z_k)$ is the same for all molecules and is given by the component divided by the number of molecules. Their definition amounts to obtain a profile similar in the shape not in the sign to a density profile. The profiles calculated by using their definition are shown in dashed (p_N-p_T) and dotted (integral) lines in Fig. 8(b). However, the inset of Fig. 8(b) shows that the definition we use takes advantage of providing a flat profile of the total reciprocal space in the bulk phases as opposed to the profile resulting from the definition of Alejandre *et al.* Fortunately, we check that the final value of the integral $\gamma^{K,1}(z_k)$ is independent of the definition used, as shown in Fig. 8(b).

IV. CONCLUSIONS

As it was underlined in the Introduction of this paper, the calculation of the surface tension of the liquid-vapor equilibrium of pure components of water, carbon dioxide, and hydrogen sulfide represents a preliminary step toward that of binary mixtures of water with H_2S and CO_2. We have established that the direct MC simulations of the liquid-vapor equilibrium of water by using the recent TIP4P/2005 model and a truncated potential give surface tension results in excellent agreement with previous simulations of MD by using a LJ potential modified by a switching function and with experiments. This result confirms the fact that in systems where long range Coulombic interactions are several orders of magnitude higher than the dispersion-repulsion energy contributions, the effects due to the discontinuities in the LJ potential become very weak. This is in contrast to the simulation of the liquid-vapor interface of *n*-alkanes.

We have also shown that the surface tension values of a less polar molecule (H_2S) and of a quadrupolar molecule (CO_2) are well reproduced with standard nonpolarizable potential models, although the potential parameters have not been fitted to surface tension values. We have also checked that the pure component phase diagrams of water, carbon dioxide, and hydrogen sulfide calculated from the direct MC method are in line with those calculated from GEMC simulations and with experiments.

We have focused on the thermodynamical equilibrium of the liquid-vapor system by analyzing the configurational temperature and the different contributions of the normal pressure. We have completed this study by calculating the different contributions to the surface tension due to the dispersion-repulsion interactions and to the various terms of the Ewald summation technique for the electrostatic interactions.

This study aims to show that the direct MC simulation method is capable to provide accurate surface tensions of pure polar and quadrupolar fluids. We are currently establishing a methodology for the calculation of the surface tension of binary water-H2S and water-CO_2 mixtures.

APPENDIX A: EXPRESSION OF THE LOCAL COMPONENTS OF THE PRESSURE TENSOR USING THE LJ POTENTIAL AND THE EWALD SUMMATION

In the case of dispersion-repulsion and electrostatic interactions calculated from the LJ potential and Ewald summation technique, respectively, the components of the pressure tensor in the IK definition become

$$p_{\alpha\beta}(z_k) = \langle \rho(z_k) \rangle k_B T \mathbf{I} + p^{\mathrm{LJ}}_{\alpha\beta}(z_k) + p^{R}_{\alpha\beta}(z_k) + p^{K,1}_{\alpha\beta}(z_k) + p^{K,2}_{\alpha\beta}(z_k), \tag{A1}$$

where the superscripts LJ, R, and K represent the contributions of the LJ interactions, the Ewald real space, and the Ewald reciprocal space, respectively. The LJ contribution to the pressure tensor can be calculated from the following expression:

$$p^{\mathrm{LJ}}_{\alpha\beta}(z_k) = -\frac{1}{A}\left\langle \sum_{i=1}^{N-1}\sum_{j=i+1}^{N}\sum_{a=1}^{N_i}\sum_{b=1}^{N_j} \frac{(\mathbf{r_{ij}})_\alpha \cdot (\mathbf{r_{iajb}})_\beta}{r_{iajb}} \frac{du_{\mathrm{LJ}}(r_{iajb})}{dr_{iajb}} \times \frac{1}{|z_{ij}|}\theta\left(\frac{z_k - z_i}{z_{ij}}\right)\theta\left(\frac{z_j - z_k}{z_{ij}}\right)\right\rangle. \tag{A2}$$

The contribution of the real space to the local pressure is given by Eq. (A3),

$$p^{R}_{\alpha\beta}(z_k) = \frac{1}{4\pi\epsilon_0 A}\left\langle \sum_{i=1}^{N-1}\sum_{j=i+1}^{N}\sum_{a=1}^{N_i}\sum_{b=1}^{N_j} q_{ia}q_{jb} \times \left(\frac{2}{\sqrt{\pi}}\alpha r_{iajb}\exp(-\alpha^2 r^2_{iajb}) + \mathrm{erfc}(\alpha r_{iajb})\right) \times \frac{(\mathbf{r_{ij}})_\alpha \cdot (\mathbf{r_{iajb}})_\beta}{r^3_{iajb}} \frac{1}{|z_{ij}|}\theta\left(\frac{z_k - z_i}{z_{ij}}\right)\theta\left(\frac{z_j - z_k}{z_{ij}}\right)\right\rangle. \tag{A3}$$

The two contributions of the reciprocal space are given by Eqs. (A4) and (A5),

Downloaded 04 Jul 2008 to 194.214.132.32. Redistribution subject to AIP license or copyright; see http://jcp.aip.org/jcp/copyright.jsp

$$p_{\alpha\beta}^{K,1}(z_k) = \frac{1}{4\pi\epsilon_0}\left\langle \frac{2\pi}{V^2}\sum_{\mathbf{h}\neq 0} H_k(z_i)Q(h)S(\mathbf{h})S(-\mathbf{h}) \times\left(\delta_{\alpha\beta} - \frac{2\mathbf{h}_\alpha\mathbf{h}_\beta}{h^2} - \frac{\mathbf{h}_\alpha\mathbf{h}_\beta}{2\alpha^2}\right)\right\rangle, \tag{A4}$$

$$p_{\alpha\beta}^{K,2}(z_k) = -\frac{1}{4\pi\epsilon_0}\left\langle \frac{2\pi}{V^2}\sum_{i=1}^{N}\sum_{a=1}^{N_a}(\mathbf{r}_{ia}-\mathbf{r}_i)_\beta q_{ia} \times\sum_{\mathbf{h}\neq 0} H_k(z_i)Q(h)i\mathbf{h}_\alpha[S(\mathbf{h})\exp(-i\mathbf{h}\cdot\mathbf{r}_{ia}) - S(-\mathbf{h})\exp(-i\mathbf{h}\cdot\mathbf{r}_{ia})]\right\rangle, \tag{A5}$$

where $H_k(z_i)$ is a top-hat function defined in Eq. (20). The total surface tension $\gamma(z)$ calculated from $\int_{-\infty}^{z_k}(p_N(z_k) - p_T(z_k))dz$ can be decomposed into the following terms: $\gamma^{LJ}(z_k)$, $\gamma^{R}(z_k)$, $\gamma^{K,1}(z_k)$, and $\gamma^{K,2}(z_k)$ calculated from Eqs. (A2)–(A5), respectively.

APPENDIX B: EXPRESSION OF THE LOCAL CONTRIBUTION TO THE SURFACE TENSION FROM THE VIRIAL ROUTE

Taking the derivative of the potential with respect to the surface allows us to express the derivative of the potential with respect to the surface as a sum of local derivatives for each z_k according to Eq. (B1),

$$\frac{\partial U}{\partial A} = \sum_k \frac{\partial U_{z_k}}{\partial A}, \tag{B1}$$

where $\partial U_{z_k}/\partial A$ can be expressed after further elaboration as in Eq. (B2),

$$\gamma_{\mathrm{KBZ}}(z_k) = \frac{\partial U_{z_k}}{\partial A}, \tag{B2}$$

$$= \sum_{i\in k}\sum_a\left\{\frac{1}{4\pi\epsilon_0}\sum_{j\neq i}\sum_b -q_{ia}q_{jb}\frac{1}{r_{iajb}}A(\mathbf{r}_{iajb},\mathbf{r}_{ij})\left[\frac{2\alpha}{\sqrt{\pi}r_{iajb}}\exp(-(\alpha^2 r_{iajb}^2)) + \frac{\mathrm{erfc}(\alpha r_{iajb})}{r_{iajb}^2}\right] + \frac{1}{V\epsilon_0}\sum_{h\neq 0}Q(h)\mathrm{Im}\left\{\left(\sum_i\sum_a \times\left[-(\mathbf{r}_i)_x\frac{\pi l}{2(L_x)^3} - (\mathbf{r}_i)_y\frac{\pi m}{2(L_y)^3} + (\mathbf{r}_i)_z\frac{\pi n}{L_xL_yL_z}\right] + A(\mathbf{h},\mathbf{r}_{ia})\right)(\exp(-i\mathbf{h}\mathbf{r}_{ia}))\left(\sum_i\sum_a\exp(i\mathbf{h}\mathbf{r}_{ia})\right)\right\} + \frac{1}{2V}\sum_{h\neq 0}\left[\frac{2\pi^2 l^2}{(L_x)^4} + \frac{2\pi^2 m^2}{(L_y)^4} - \frac{4\pi^2 n^2}{L_xL_y(L_z)^2}\right]\frac{1}{h^4}\exp\left(-\frac{h^2}{4\alpha^2}\right)\left[\frac{h^2}{4\alpha^2}+1\right]S(\mathbf{h})S(-\mathbf{h}) - \sum_{j\neq i}\sum_b\frac{1}{r_{iajb}}A(\mathbf{r}_{iajb},\mathbf{r}_{ij})\frac{48\epsilon_{ij}}{r_{iajb}}\left[\left(\frac{\sigma_{ij}}{r_{iajb}}\right)^{12} - \frac{1}{2}\left(\frac{\sigma_{ij}}{r_{iajb}}\right)^6\right]\right\}, \tag{B3}$$

where the function $A(\mathbf{u},\mathbf{v})$ is defined as

$$A(\mathbf{u},\mathbf{v}) = \left((\mathbf{u})_x\frac{(\mathbf{v})_x}{4L_x^2} + (\mathbf{u})_y\frac{(\mathbf{v})_y}{4L_y^2} - (\mathbf{u})_z\frac{(\mathbf{v})_z}{2L_yL_x}\right) \tag{B4}$$

and Im denotes the imaginary part of the complex variable. The local versions $\gamma_{\mathrm{TA}}(z_k)$ and $\gamma_{\mathrm{KBZ}}(z_k)$ can be compared to the standard local version $\gamma_{\mathrm{IK}}(z_k)$ and allow us to check the features of the profile of the surface tension calculated from the new approach TA and the well-known approach of Kirkwood and Buff. In fact, the local version of the surface tension using the KBZ approach can be considered as the local version of the Kirkwood and Buff definition.

[1] *IPCC Special Report on Carbon Dioxide Capture and Storage* (Cambridge University Press, Cambridge, 2005).
[2] A. Hebach, A. Oberhof, N. Dahmen, A. Kogel, H. Ederer, and E. Dinjus, J. Chem. Eng. Data **47**, 1540 (2002).
[3] C. S. Herrick and G. L. Gaines, Jr., J. Phys. Chem. **77**, 2703 (1975).
[4] G. S. Strathdee and R. M. Given, J. Phys. Chem. **80**, 1714 (1976).
[5] D. B. MacLeod, IEEE Trans. Plasma Sci. **19**, 38 (1923).
[6] C. F. Weinaug and D. L. Katz, Ind. Eng. Chem. **35**, 239 (1943).
[7] E. A. Guggenheim, J. Chem. Phys. **13**, 253 (1945).
[8] Y.-X. Zuo and E. H. Stenby, Can. J. Chem. Eng. **75**, 1130 (1997).
[9] J. S. Rowlinson, J. Stat. Phys. **20**, 197 (1979).
[10] J. W. Cahn and J. E. Hilliard, J. Chem. Phys. **28**, 258 (1958).
[11] V. Bongiorno, L. E. Scriven, and H. T. Davis, J. Colloid Interface Sci. **57**, 462 (1976).
[12] A. J. M. Yang, P. D. I. Fleming, and J. H. Gibbs, J. Chem. Phys. **64**, 3732 (1976).
[13] A. Trokhymchuk and J. Alejandre, J. Chem. Phys. **111**, 8510 (1999).
[14] C. Ibergay, A. Ghoufi, F. Goujon, P. Ungerer, A. Boutin, B. Rousseau, and P. Malfreyt, Phys. Rev. E **75**, 051602 (2007).
[15] J. Alejandre, D. J. Tildesley, and G. A. Chapela, J. Chem. Phys. **102**, 4574 (1995).
[16] S. E. Feller, R. W. Pastor, A. Rojnuckarin, S. Bogusz, and B. R. Brooks, J. Chem. Phys. **100**, 17011 (1996).
[17] B. Shi, S. Sinha, and V. K. Dhir, J. Chem. Phys. **124**, 204715 (2006).
[18] F. Goujon, P. Malfreyt, J. M. Simon, A. Boutin, B. Rousseau, and A. H. Fuchs, J. Chem. Phys. **121**, 12559 (2004).
[19] J. L. F. Abascal and C. Vega, J. Chem. Phys. **123**, 234505 (2005).
[20] C. Vega and E. de Miguel, J. Chem. Phys. **126**, 154707 (2007).
[21] J. G. Harris and K. H. Yung, J. Phys. Chem. **99**, 12021 (1995).
[22] T. Kristof and J. Liszi, J. Phys. Chem. B **101**, 5480 (1997).
[23] M. P. Allen and D. J. Tildesley, *Computer Simulation of Liquids* (Clarendon, Oxford, 1989).
[24] E. R. Smith, Proc. R. Soc. London, Ser. A **375**, 475 (1981).
[25] D. M. Heyes, Phys. Rev. B **49**, 755 (1994).
[26] J. Kolafa and J. W. Perram, Mol. Simul. **9**, 351 (1992).
[27] M. Guo and B. C. Y. Lu, J. Chem. Phys. **106**, 3688 (1997).
[28] F. Goujon, P. Malfreyt, A. Boutin, and A. H. Fuchs, J. Chem. Phys. **116**, 8106 (2002).
[29] B. Efron, *The Jackknife the Boostrap and other Resampling Plans* (SIAM, Philadelphia, 1982).
[30] J. S. Rowlinson and B. Widom, *Molecular Theory of Capillarity* (Clarendon, Oxford, 1982).
[31] J. G. Kirkwood and F. P. Buff, J. Chem. Phys. **17**, 338 (1949).
[32] J. H. Irving and J. G. Kirkwood, J. Chem. Phys. **18**, 817 (1950).
[33] J. P. R. B. Walton, D. J. Tildesley, J. S. Rowlinson, and J. R. Henderson, Mol. Phys. **48**, 1357 (1983).

Downloaded 04 Jul 2008 to 194.214.132.32. Redistribution subject to AIP license or copyright; see http://jcp.aip.org/jcp/copyright.jsp

[34] J. P. R. B. Walton, D. J. Tildesley, and J. S. Rowlinson, Mol. Phys. **58**, 1013 (1986).
[35] G. J. Gloor, G. Jackson, F. J. Blas, and E. Miguel, J. Chem. Phys. **123**, 134703 (2005).
[36] A. Ghoufi, F. Goujon, V. Lachet, and P. Malfreyt, Phys. Rev. E **77**, 031601 (2008).
[37] E. M. Blokhuis, D. Bedeaux, C. D. Holcomb, and J. A. Zollweg, Mol. Phys. **85**, 665 (1995).
[38] A. J. C. Ladd and L. V. Woodcok, Mol. Phys. **2**, 611 (1978).
[39] J. R. Errington and D. A. Kofke, J. Chem. Phys. **127**, 174709 (2007).
[40] P. Orea, J. Lopez-Lemus, and J. Alejandre, J. Chem. Phys. **123**, 114702 (2005).
[41] A. Z. Panagiotopoulos, Mol. Phys. **61**, 812 (1987).
[42] A. E. Ismail, G. S. Grest, and M. J. Stevens, J. Chem. Phys. **125**, 014702 (2006).
[43] J. L. Rivera, F. W. Starr, P. Paricaud, and P. T. Cummings, J. Chem. Phys. **125**, 094712 (2006).
[44] F. Chen and P. E. Smith, J. Chem. Phys. **126**, 221101 (2007).
[45] W. L. Jorgensen, J. Chandrasekhar, J. D. Madura, R. W. Impey, and M. L. Klein, J. Chem. Phys. **79**, 926 (1983).
[46] Data taken from the saturation properties of water, carbon dioxide, and hydrogen sulfide at the http://webbook.nist.gov.
[47] C. Nieto-Draghi, T. de Bruin, J. Pérez-Pellitero, J. Bonet Avalos, and A. D. Mackie, J. Chem. Phys. **126**, 064509 (2007).
[48] R. L. Rowley, W. V. Wilding, J. L. Oscarson, N. A. Tundel, T. L. Marshall, T. E. Daubert, and R. P. Danner, *DIPPR Data Compilation of Pure Compound Properties: Design Institute for Physical Properties* (AIChE, New York, 2002).
[49] H. H. Rugh, Phys. Rev. Lett. **78**, 772 (1997).
[50] O. G. Jepps, G. Ayton, and D. J. Evans, Phys. Rev. E **62**, 4757 (2000).
[51] G. Rickayzen and J. G. Powles, J. Chem. Phys. **114**, 4333 (2001).
[52] J. Delhommelle and D. J. Evans, J. Chem. Phys. **114**, 6229 (2001).

Downloaded 04 Jul 2008 to 194.214.132.32. Redistribution subject to AIP license or copyright; see http://jcp.aip.org/jcp/copyright.jsp